J. Mol. Biol. (1995) **247**, 111–124

JMB

Crystal Structure of the Closed Form of Chicken Cytosolic Aspartate Aminotransferase at 1.9 Å Resolution

Vladimir N. Malashkevich[1]*, Boris V. Strokopytov[2] Vsevolod V. Borisov[2], Zbigniew Dauter[3], Keith S. Wilson[3] and Yurii M. Torchinsky[1]

[1]*Institute of Molecular Biology, Academy of Sciences of the Russia, Vavilova street 32, 117984 Moscow, Russia*

[2]*Institute of Crystallography Academy of Sciences of the Russia, Leninsky prospect 59 117333 Moscow, Russia*

[3]*EMBL Oustation, Notkestrasse 85, 22603 Hamburg, Germany*

**Corresponding author*

The crystal structure of chicken cytosolic aspartate aminotransferase (cAATase; EC 2.6.1.1) has been solved and refined at 1.9 Å resolution. Orthorhombic crystals, space group $P2_12_12_1$, a = 56.4 Å, b = 126.0 Å and c = 142.3 Å, were grown from polyethylene glycol solutions in the presence of maleate, a dicarboxylic inhibitor that forms a Michaelis-like complex. The pyridoxal form of the enzyme was used for crystallization. Diffraction data were collected using synchrotron radiation. The structure of the new orthorhombic crystal form was solved by molecular replacement using the partially refined 2.8 Å resolution structure of the high-salt crystal form as a search model. The final value of the crystallographic *R*-factor after rigid body and restrained least-squares refinement is 0.175 with very good model geometry. The two 2-fold-related subunits of cAATase have distinct environments in the crystal lattice. Domain movement is strictly hindered by the lattice contacts in one subunit, while the second one possesses conformational freedom. Despite their different environments, both subunits were found in the closed conformation with one maleate molecule tightly bound in each active site. The present study allows a detailed comparison of the highly refined structures of the aspartate aminotransferase isozymes, and thus provide better insight into the role of conserved and variable residues in substrate recognition and catalysis.

Keywords: X-ray structure; aspartate aminotransferases; closed form; inhibitor complex

Introduction

Aspartate aminotransferase (AATase; EC 2.6.1.1) catalyzes the reversible interconversion of dicarboxylic amino and keto acids. Its catalytic activity is dependent on tightly bound pyridoxal-5'-phosphate (PLP) as coenzyme, which alternates between aldehyde and amine forms in the two half-reactions constituting a catalytic cycle:

L-Aspartate + PLP-enzyme ⇌ oxalacetate + PMP-enzyme

2-Oxoglutarate + PMP-enzyme ⇌ L-glutamate + PLP-enzyme

The reaction mechanism is complex, with eight distinct kinetic steps per half-reaction being spectroscopically detectable in rapid reaction studies (Fasella & Haslam, 1967). Despite the complexity of the reaction mechanism, AATase is presently one of the best understood enzymes, due to the wealth of crystallographic information accumulated to date (Jansonius & Vincent, 1987). High and medium-resolution structures of mitochondrial and cytosolic AATases from chicken (Ford *et al*., 1980; McPhalen *et al*., 1992*a*; Borisov *et al*., 1985; Harutyunyan *et al*., 1985), pig heart (Arnone *et al*., 1985; Izard, 1990), and of *Escherichia coli* AATase (Smith *et al*., 1989; Okamoto, 1994; Jäger *et al*., 1994) are available. Additionally, the structures of several inhibitor and

Present addresses: Vladimir N. Malashkevich, Biozentrum der Universität Basel, Klingelbergstrasse 70, CH-4056 Basel, Switzerland; Y. M. Torchinsky, The Institutes for Applied Research, Ben-Gurion University of Negev, P.O.B. 1025, Beer-Sheva 84110, Israel.

Abbreviations used: AATase, aspartate aminotransferase; PLP, pyridoxal-5'-phosphate; PMP, pyridoxamine-5'-phosphate; eAATase, *E. coli* AATase; CAATase, mAATase, cytosolic and mitochondrial isozymes of AATase; PEG, polyethylene glycol 4000; F_{obs} and F_{calc}, observed and calculated structure factors.

0022–2836/95/110111–14 $08.00/0

Table 1

Data collection and refinement statistics for cAATase

Resolution range (Å)	6.0–1.9	Side-chains	21.1
Reflections:		Entire molecule	18.6
Observed	310,873	Water molecules	41.6
Unique	69,643	r.m.s. deviations from	
Completeness (%)	98.5	ideal geometry:	
R_{sym}[a]	0.095	Bond distances (Å)	0.010
R-factor[b]	0.175	Bond angles (deg.)	1.9
Number of atoms:		Torsion angles (deg.)	23.3
Protein	6506	Planar groups (Å)	0.011
Solvent	768	Bad contacts (Å)	0.008
Mean B-factor (Å^2):		r.m.s. coordinate error (Å)[c]	0.24
Main chain	16.2		

[a] $R_{sym} = \Sigma_{hkl}\Sigma_i|\langle I(hkl)\rangle - I(hkl)_i| / \Sigma_{hkl}\Sigma_i I(hkl)_i$, and $\langle I(hkl)\rangle$ is the average of I_i over all symmetry equivalents.

[b] $R = \Sigma_{hkl}|F(hkl)_{obs} - F(hkl)_{calc}| / \Sigma_{hkl}F(hkl)_{obs}$.

[c] Estimated using the program SIGMAA (Read, 1986).

substrate complexes have been solved, providing structural models of virtually all obligatory intermediates (Kirsch *et al*., 1984; Jansonius & Vincent, 1987; Jäger *et al*., 1994; Malashkevich *et al*., 1993; J. N. Jansonius *et al*., unpublished results). In addition to a long history of classical solution studies (for a review, see Christen & Metzler, 1985), more recent site-directed mutagenesis analyses, capitalizing on the X-ray crystallographic successes, have delineated the mechanistic roles of most active site residues (Malcolm & Kirsch, 1985; Cronin & Kirsch, 1988; Toney & Kirsch, 1987, 1991; Goldberg *et al*., 1991; Kuramitsu *et al*., 1991; Hayashi *et al*., 1991; Inoue *et al*., 1991; Ziak *et al*., 1993).

cAATase from chicken heart is an α_2 dimer with 411 amino acid residues per subunit (M_r $2 \times 46{,}500$). Each subunit binds one molecule of PLP through an aldimine linkage to the ϵ-amino group of Lys258. Chicken heart cAATase shares 85% sequence identity with other cAATases (Graf-Hausner *et al*., 1983), while there is only 45 to 50% sequence identity between the cytosolic and mitochondrial AATases, and only 40% between the mammalian and *E. coli* enzymes (Mehta *et al*., 1989). Crystallographic studies at high resolution of chicken cAATase were temporarily hampered by the only moderate resolution attainable from the crystals grown from ammonium sulfate solutions (about 2.7 to 2.8 Å; Borisov *et al*., 1985; Harutyunyan *et al*., 1985). Extensive crystallization experiments resulted in several new crystal forms from polyethylene glycol (PEG) solutions (Malashkevich & Sinitzina, 1991). The best one, obtained by cocrystallization of the PLP-enzyme with the non-covalent inhibitor maleate, has drastically improved diffraction quality compared with the original crystals and was used for data collection at the synchrotron beam at EMBL Outstation, DESY, Hamburg. Here, we report the X-ray crystal structure of the maleate complex of chicken cAATase refined at 1.9 Å resolution. Comparison of this highly refined structure with those of homologous aspartate aminotransferases, which exhibit somewhat different catalytic properties and substrate specificities, should provide a deeper insight into the mechanism of enzymatic transamination.

Results and Discussion

Overall quality of the structure

The refined model of cAATase contains 6506 non-hydrogen protein atoms, two covalently bound molecules of PLP and two maleate molecules. Additionally, 768 water molecules were included (Table 1). Almost all amino acid residues were found to have good electron densities in the final $(2F_{obs} - F_{calc})$, α_{calc} map. The amino-terminal Ala2 and the carboxy-terminal Gln412 in both subunits as well as some partially or completely disordered side-chains on the surface of the protein could not be remodelled due to the lack of clear electron density. The A subunit (as defined in the PDB coordinate file) displays generally better density and has a lower overall B-factor. This is apparently due to the tighter crystal contacts in this subunit. Most of the problems with positioning side-chains were encountered in the subunit B, which forms fewer crystal contacts and consequently displays greater flexibility, as reflected in a higher overall B-factor. The segments of the structure that have highest flexibility in the subunit B (Figure 1) belong to the small domain (see below for definition); for example, flexible regions comprising residues 338 to 346 and 404 to 410. In addition to those, two external loops around positions 85 and 165 also have higher B-factors than in the subunit A. The segments of the polypeptide chain with the lowest B-factors belong to the core of the protein and to the active-site area.

The quality of the structure can be assessed by the overall coordinate error provided by the Luzzati plot (Luzzati, 1952) or calculated with the program SIGMAA (Read, 1986). The methods give similar values of 0.22 Å and 0.24 Å, respectively. The value of the co-ordinate error is not uniform through the unit cell (Cruickshank, 1967), but displays an

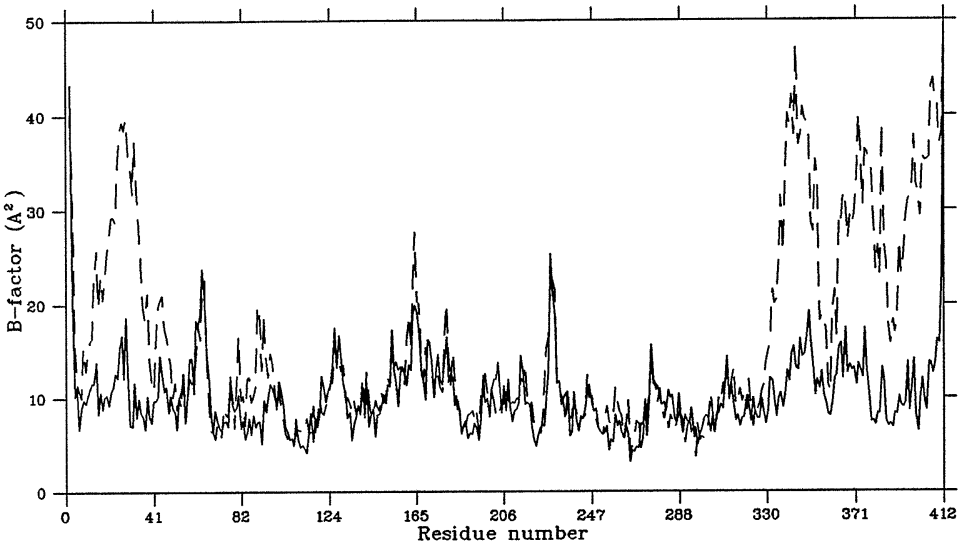

Figure 1. Variation of the *B*-factors (average for the main-chain atoms) along the polypeptide chain. Continuous line, subunit A; broken line, subunit B. The drastic difference between the *B*-factor distributions in the small domain area (residues 2 to 48 and 326 to 412) is due to the highly asymmetric crystal contacts formed by the 2 subunits. Subunit A is well fixed due to the numerous lattice contacts, while the small domain of subunit B lacks close contacts and, therefore, its behavior resembles more closely that in solution.

obvious correlation with the local *B*-factors. Therefore, the coordinate error for the more rigid active site area is as low as 0.10 Å (overall *B*-factor is 9.8 Å^2) in subunit A, and 0.12 Å (overall *B*-factor is 12.7 Å^2) in subunit B.

A plot of the main-chain torsion angles (Ramakrishnan & Ramachandran, 1965) illustrates that most of the residues lie in the conformationally allowed regions (Figure 2). The non-glycine residues that have unfavorable ϕ, ψ angles are the same in both subunits: Ser296 (74°, – 62°) is located at the subunit interface close to the active site, Asn127 (58°,38°), Phe183 (78°,0°), Cys216 (59°,39°), His378 (64°,33°) only marginally outside the allowed conformational region, are located in surface loops that may adopt a specific conformation due to the high degree of hydration. In the B subunit four additional residues (Thr335, Glu336, Ser339 and Leu397) lie slightly outside the allowed region, but they all belong to the poorly defined flexible part of the small domain and their conformations could not be determined with great accuracy. Two proline residues (Pro138 and Pro195) were found in the *cis*-conformation, a feature observed in all AATase crystal structures solved so far (Jansonius & Vincent, 1987; Jäger *et al*., 1994; Arnone *et al*., 1985).

In total, 92% of all non-glycine residues are in the ''core'' region of the Ramachandran plot (Morris *et al*., 1992). The estimated standard deviation of the χ_1 angles from the allowed g^-, T and g^+ conformations (excluding 40 proline residues) is 16.5°. The average (standard deviation) H-bond energy over the entire molecule is $-1.9(\pm 0.74)$ kcal / mol. This places the refined cAATase structure in the good to excellent group as defined by Morris *et al*. (1992).

Subunit and domain structure

cAATase, like all other AATases, is an α_2 dimer in which the two subunits form an extensive interface

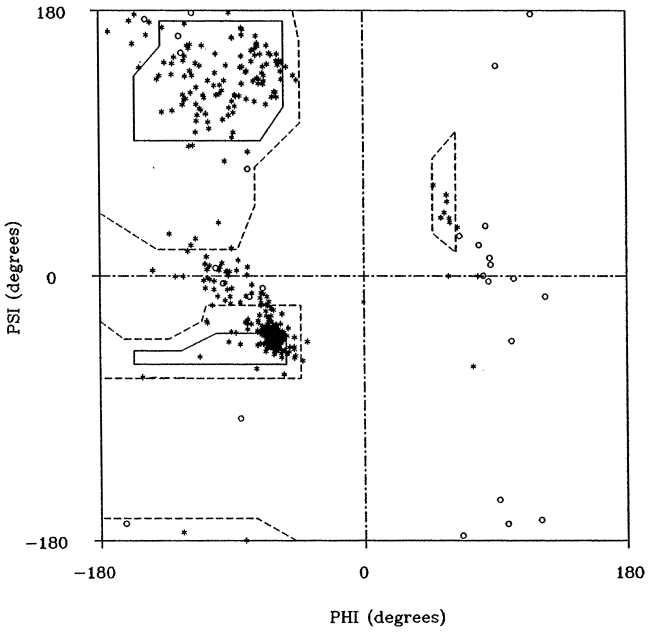

Figure 2. ϕ, ψ plot of the refined structure of the maleate complex of cAATase (only subunit A is shown). Glycine residues are labeled with open circles and non-glycine residues are labeled with asterisks (*). Only a few non-glycine residues fall out of the allowed conformational areas. The possible reasons for this are discussed in the text.

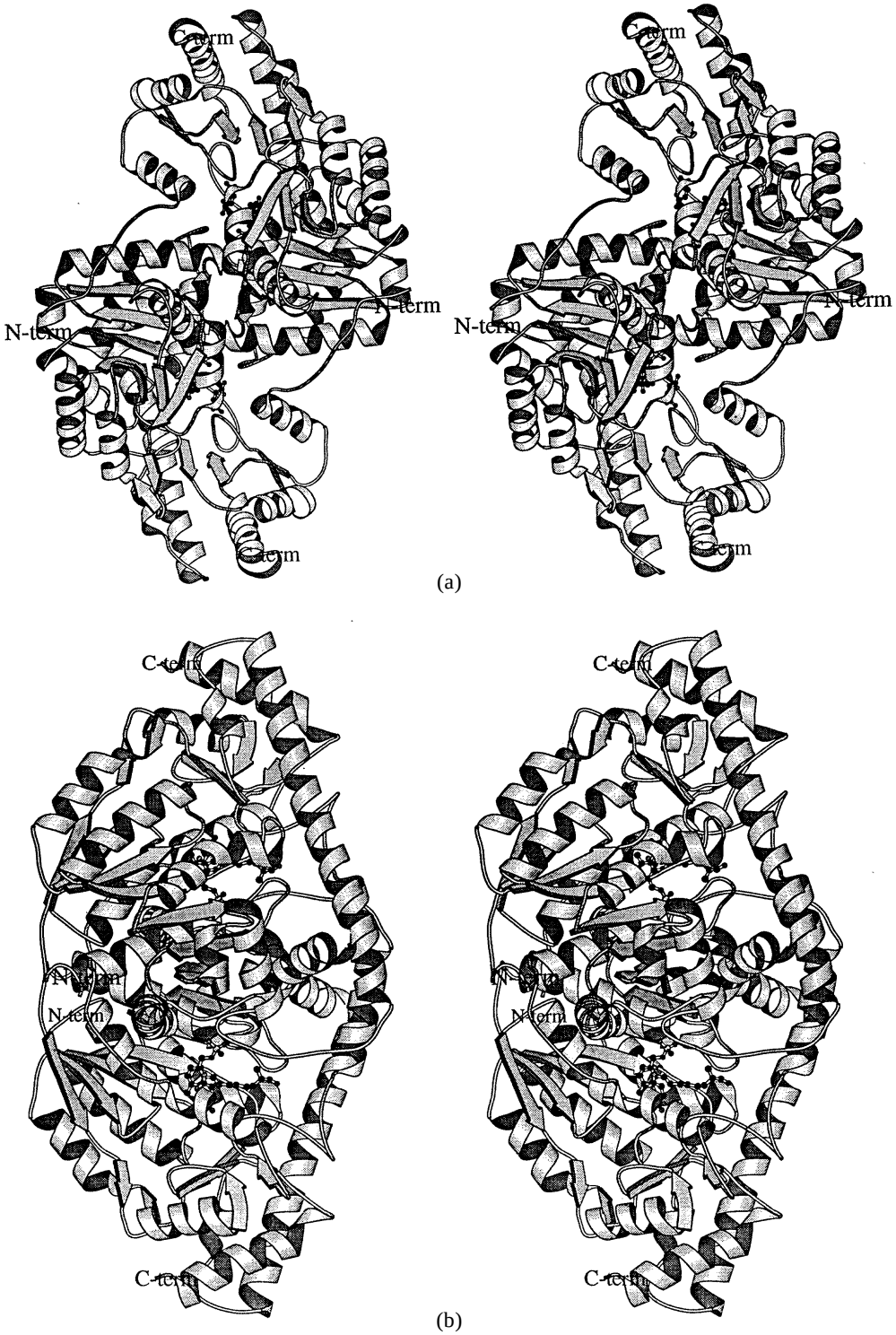

Figure 3. Stereoviews of the maleate complex of cAATase. (a) View along the non-crystallographic 2-fold axis. (b) View perpendicular to the non-crystallographic 2-fold axis. Ball-and-stick models show the positions of PLP and maleate in the 2 active sites of the dimer. Subunits A (on the top) and B (below) have an extensive area of contact, passing through both active sites, around the local 2-fold axis.

(see Figure 3). Each subunit can be divided into two functional domains (Figure 4). This division was initially quite arbitrary at the domain interface (Ford *et al*., 1980), but after the inhibitor studies of mAATase revealed a correlated motion of the amino (residues 10 to 48) and carboxy-terminal (residues 326 to 412) parts of the polypeptide chain upon inhibitor binding, this part of the structure was redefined as the small domain (Jansonius & Vincent, 1987; McPhalen *et al*., 1992*b*). The large domains (residues 49 to 325) form the central, most rigid, part of the cAATase dimer and contribute largely to the

interactions between subunits. The amino-terminal arm (residues 2 to 10) protrudes from the small domain of one subunit and forms a number of additional contacts with the large domain of the adjacent subunit.

Subunit and domain interfaces

The total water-accessible surface area of the dimer is 29,479 Å^2, while the intersubunit interface is 3710 Å^2, i.e. about one-eighth of the total dimer surface. The subunits are tightly associated *via* numerous interactions between their large domains and *via* interactions of the amino-terminal arm of one subunit with the large domain of the second subunit (Figure 3(a)). Maleate and coenzyme also contribute to the intersubunit contacts by interacting with the residues from both subunits. The subunits form a total of 157 non-hydrogen atom to atom contacts with a 3.5 Å cutoff including 55 hydrogen bonds and eight

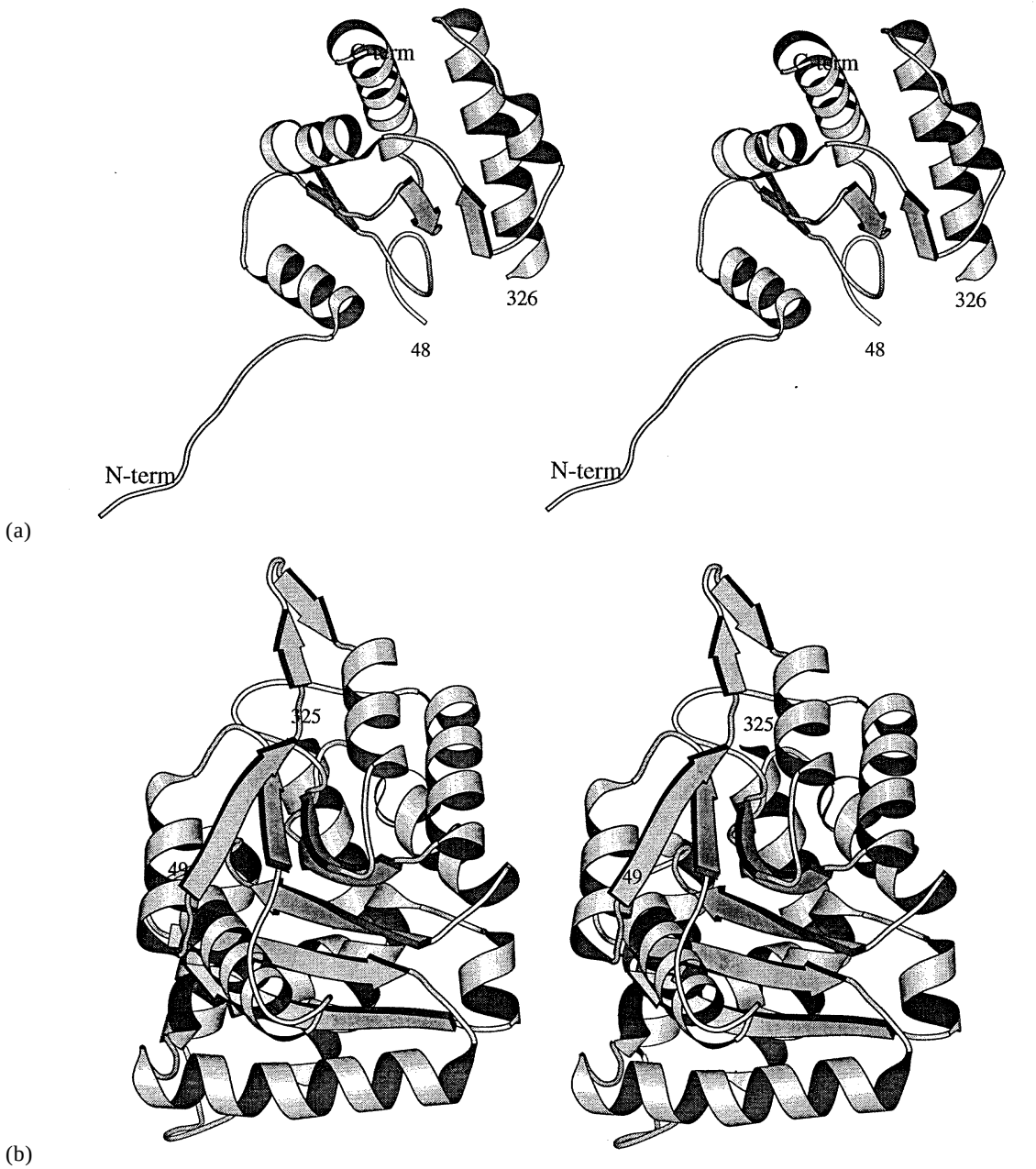

Figure 4. Stereoviews of the small and the large domains of cAATase. (a) Small domain. The N-terminal and C-terminal parts of the polypeptide chain form together a globular structure that was observed to undergo a concerted movement upon binding dicarboxylic substrates and inhibitors (Jansonius & Vincent, 1987). Rotation occurs around a hinge between residues 325 and 326. The first 6 residues of the N-terminal arm do not take part in this movement due to tight contacts with the surface of the large domain of the adjacent subunit (see Figure 3(a)). (b) Large domain. The 7-stranded β-pleated sheet forms the core of the domain. Two extensive hydrophobic clusters lie on both sides of the sheet (see also Table 4).

Table 2

Subunit and domain interface residues in cAATase

A. *Subunit interface*
Ala2, Ser4 to Ala7, Val9, Pro10, Ala12 to Val15, Phe18, Arg41, Pro47, Glu57, Gln58, Ala61, His68 to Tyr70, Ile73, Leu106, Arg113, Trp122, Glu141, Asn 142, Ser145, Asp149, Phe218, Glu249, PLP258[a], Gly261, Tyr263 to Arg266, Asn279, Arg282, Ser285, Gln286, Glu288, Arg292, Thr293, Trp295 to Pro299, Ser300, Gln301, MA1414[a]

B. *Domain interface*
Small domain
Pro10, Ala12 to Val15, Phe18, Ala39 to Arg41, Pro47, Trp48, Met326 to Arg329, Thr349, Gln356, Ile357, Met359, Phe360, Phe362, Arg386

Large domain
Leu50, Pro51, Glu69, Ile73, Trp122, Trp140, Arg166, Asn194 to Thr198, Tyr225, Phe228, PLP258, Tyr263, Ser285, Gln286, Glu288, Arg292, Asn322, Val323 to Thr325

[a] PLP258 and MAL414 denote Lys258-PLP aldimine and maleate, respectively. Both groups belong to the subunit and domain interfaces.

salt bridges. Coenzyme and maleate contribute to three intersubunit hydrogen bonds (Table 2).

The interface between the domains is similarly complex. In addition to a double polypeptide link there are many other interactions and these are listed in Table 3. The domains form 166 non-bonded interactions (3.5 Å cutoff) including 22 hydrogen bonds and four salt bridges.

Assignment of the secondary structure

The secondary structure assignment was done with the program DSSP (Kabsch & Sander, 1983) and corrected at some α-helix and β-strand termini where alternative assignments are possible (Table 3). One subunit of cAATase contains 15 α-helices that are numbered in order of their position along the polypeptide chain. The helices vary in length from five residues (helix 4) to 32 residues (helix 13). Nine out of 15 helices have some irregularities in their hydrogen-bonding pattern. Helix 9 is actually split into two parts by a 61° bend (as applied to the helix axis) at Ala237; helix 11 has a gradual bend of 19°; helix 13 has a 7° bend at Lys324. Three 4-turns are detected in addition to the helices described above.

Four β-sheets are assigned on the basis of hydrogen-bonding patterns and main-chain torsion angles. A small double-stranded parallel structure, A, and antiparallel structure, D, belong to the small

Table 3

Secondary structure assignments in cAATase

Structure	Residues
α-Helices[a]	(1) Ala16 to Glu26, (2) Pro51 to Gly62, (3) Pro77 to Leu88, (4) Pro93 to Gln97, (5) Gly107 to Trp122, (6) Glu141 to Ala150, (7) Leu170 to Lys179, (8) Pro202 to Arg215, (9) Leu233 to Glu246, (11) Glu277 to Thr294, (12) Ser300 to Thr311, (13) Pro313 to Leu344, (14) Asn351 to Asp355, (15) Pro367 to Lys377, (16) Asn396 to Ile411
4-Turns[b]	Ala163 to Arg166, Phe228 to Gly231, Ser256 to Phe260
β-Turns[c]	
Type I	Ser4 to Ala7; Phe6 to Val9; Asp29 to Lys32; Thr42 to Gly45; Asp63 to Leu66; Pro72 to Gly75; Gly89 to Ser92; Asn128 to Thr131; Asp162 to Lys165; Met382 to Gly385
Type II	Pro181 to Ser184; Tyr225 to Phe228
β-Strands[d]	
Large domain	(B1) Val100 to Leu106; (B2) Val133 to Ser136; (B3) Asp154 to Tyr158; (C1) Trp161 to Asp162; (C2) Gly167 to Leu168; (B4) Ile185 to His189; (B5) Phe218 to Ser223; (B6) Leu250 to Ser255; (B7) Val267 to Val273;
Small domain	(A1) Val33 to Asn 34; (D1) Phe360 to Phe362; (A2) Ile379 to Tyr380; (D2) Arg386 to Asn388

The secondary structure assignment is given only for subunit S1. In subunit S2 there are few minor differences at the termini of the secondary structure elements.

[a] The numbering of helices has been kept as for mAspAT (Jansonius *et al*., 1985) for consistency. Helix 10 is omitted. Helices 6, 7, 14 and 16 are interrupted by irregularities in hydrogen-bonding pattern. Helices 1, 5, 8, 11 and 13 have 1 or more internal hydrogen bonds missed. Helix 9 is actually split into 2 parts by a 61° bend at Ala237; helix 11 has a gradual bend of 19°; helix 13 has a 7° bend at Lys324.

[b] Irregular α-helical turns with hydrogen bond from i to $i + 4$.

[c] Turn types as defined by Crawford *et al*. (1973).

[d] Strands are labeled in order of position in sequence in the corresponding β-structures.

Table 4

Hydrophobic clusters in cAATase

A. *Large domain*

Cluster I
Leu74, Val103, Leu112, Ile114, Phe118, Leu119, Val133, Val135, Val146, Phe147, Phe152, Ile155, Ile185, Ile187, Phe218, Phe220, Phe251, Leu270, Val272, Val280, Val283, Leu284, Met287

Cluster II
Leu88, Ile95, Val100, Tyr158, Leu168, Leu170, Leu173, Leu174, Met177, Phe186, Leu188, Pro200, Trp205, Ile208, Val211, Met212, Leu217, Pro219, Phe221, Val240, Phe243, Val244, Phe248, Leu250, Val273

Cluster III
Tyr40, Trp48, Leu50, Val52, Val53, Val56, Phe79, Ile86, Phe228, Leu233, Phe256, Phe260, Leu262, Val267, Ile305, Val306, Leu310, Leu315, Phe316, Trp319, Met326, Met359

B. *Small domain*

Cluster IV
Val33, Leu35, Leu337, Leu341, Trp350, Ile353, Leu365, Met373, Ile379, Leu381, Ile387, Met389, Leu392, Leu397, Val400, Ala401, Ile404, Val408

C. *Domain interface*

Cluster V
Val15, Phe18, Ala36, Val37, Tyr70*, Ile73, Tyr263, Met382

domain. They do not interact with each other and their β-strand orientations are almost perpendicular (Figure 4(a)). Sheets B and C belong to the large domain (Figure 4(b)). While the antiparallel sheet C is actually only an extension of a β-turn, the seven-stranded sheet B comprises 74% of the total β-structure in cAATase. Its topology (Richardson, 1981) is [+5*x*, +1*x*, –2*x*, –1*x*, –1*x*, –1] as first described by Ford *et al*. (1980) for the mitochondrial isozyme, and it is the basic element of the α/β-sandwich structure that forms the core of the large domain. Most of the β-turns are defined as type I (Crawford *et al*., 1973) and only two belong to type II.

Hydrophobic clusters

In addition to the secondary and supersecondary structure elements, hydrophobic clusters make major contributions to protein stability. Five hydrophobic clusters of different size can be found in the cAATase subunit (Table 4). Clusters I and II are adjacent to the concave and convex faces of the β-pleated sheet B of the large domain (see Jansonius *et al*., 1985), respectively. Cluster III is located mainly in the large domain, but includes a few residues from the small domain. Cluster IV forms the core of the small domain, and the small cluster V is situated in the domain interface. The existence of independent hydrophobic cores in the small and large domains of cAATase suggests that they indeed represent separate folding units.

Structure of the active site

The high quality of the electron density (Figure 5) allowed an unambiguous and accurate positioning of all groups in the active site of cAATase. Multiple interactions of the coenzyme with the active-site groups explain the low dissociation constant of PLP, 0.15 μM (Christen & Metzler, 1985). The coenzyme is covalently attached to the enzyme *via* an aldimine bond with Lys258 (Figure 6(a)). The O-3' atom is hydrogen bonded to $N^{\delta 1}$ of Asn194 (see Table 5 for distances). The phenolic oxygen atom of Tyr225, described as a hydrogen-bonding partner of O-3' in mAATase (Jansonius & Vincent, 1987), is 3.7 Å away from O-3'. The pyridine ring nitrogen atom forms a short hydrogen bond (2.6 Å) to $O^{\delta 1}$ of Asp222. The latter residue is involved in the ''charge-relay'' system (Metzler, 1979) that includes His143 and Thr139. NMR data indicate that there is a mutual nuclear Overhauser effect between the peaks assigned to the pyridine ring nitrogen atom and His143 (Kintanar *et al*., 1991). An analogous triad is of crucial importance in serine proteinases, but site-directed mutagenesis experiments with eAATase indicate that, while the negative charge on Asp222 plays a critical role in the AATase catalysis (Yano *et al*., 1992), the triad itself seems not to be important (Yano *et al*., 1991). The phosphate group of PLP is involved in a total of nine hydrogen bonds that strictly fix its position. The prevalence of the hydrogen-donating groups in the phosphate-binding pocket correlates the NMR data (Martinez-Carrion, 1975; Schnackerz, 1984; Schnackerz *et al*., 1989) that indicate the presence of two negative charges on the phosphate group. Maleate perfectly fits into the substrate-binding site by forming several favorable interactions (Figure 6(b)). One carboxylate group forms a hydrogen bond/ion pair interaction with the guanidinium group of Arg292*, $N^{\epsilon 1}$ of Trp140 and two water molecules, while the other one forms a

hydrogen bond/ion pair interaction with the guanidinium group of Arg386, $N^{\delta 1}$ of Asn194, $N^{\epsilon 1}$ of Trp140 and N of G38. In both cases the carboxylate groups form an ''end-on symmetric'' interaction, one of the seven lowest-energy types of carboxylate/guanidinium interactions found in proteins (Mitchell *et al*., 1992).

Structural differences between the subunits

The asymmetric unit of the cAATase crystals described here contains one dimer of the protein, such that the two subunits form different packing contacts. Subunit A forms nine hydrogen-bonded and 155 van der Waals lattice contacts, while subunit B forms seven hydrogen bonds and 107 van der Waals contacts. The difference becomes more pronounced when only the small domain is considered. The small domain of subunit A forms three hydrogen bonds and 63 van der Waals contacts with symmetry-related molecules in the lattice, while the small domain of subunit B forms only one hydrogen bond. The conformational freedom of subunit B was already indicated by an increased average *B*-factor relative to subunit A (Figure 1). When subunits A and B are superimposed using all 411 C^{α} atoms, they show a root-mean-square (r.m.s.) deviation of 0.4 Å. The spherical polar angles describing the transformation from subunit A to subunit B ($\omega = 90.93°$, $\phi = -10.24°$ and $\chi = 179.77°$) indicate that approximate 2-fold axis is about 1° off the *xy*-plane. If only the large or small domains are used for the superposition, the r.m.s. deviations are 0.19 Å and

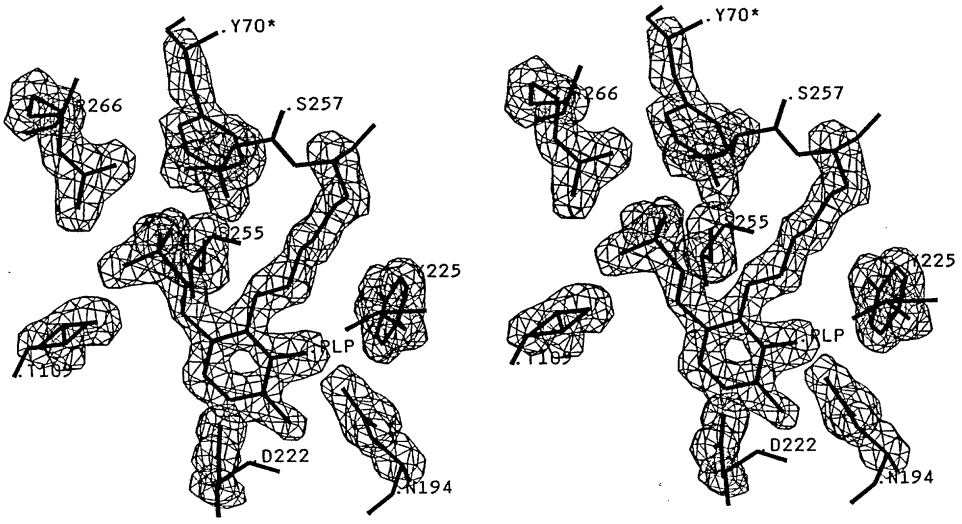

(a)

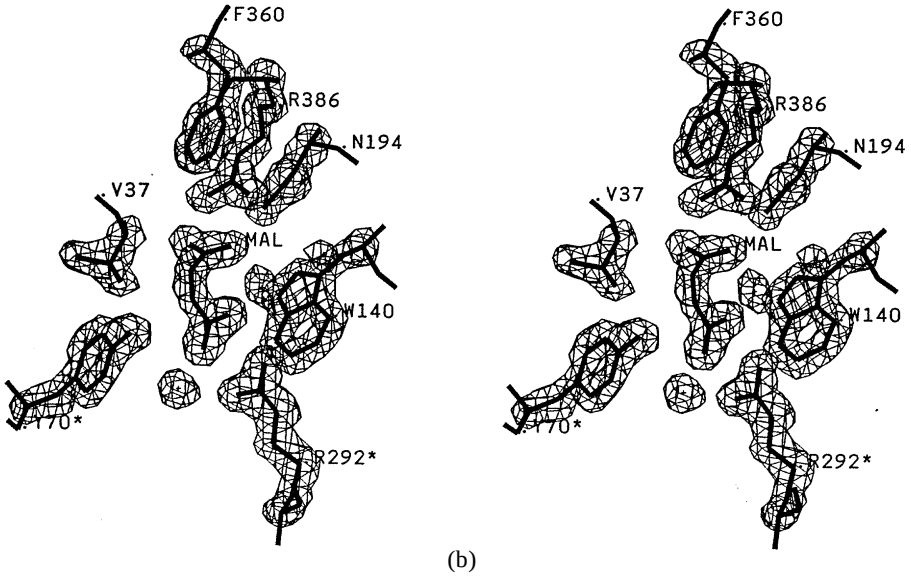

(b)

Figure 5. Electron density in the active site of cAATase. The sharp electron density allows unambigous and precise positioning of all groups in the active site. Central holes are observed in the vast majority of the aromatic rings. (a) PLP-binding area. (b) Inhibitor-binding area.

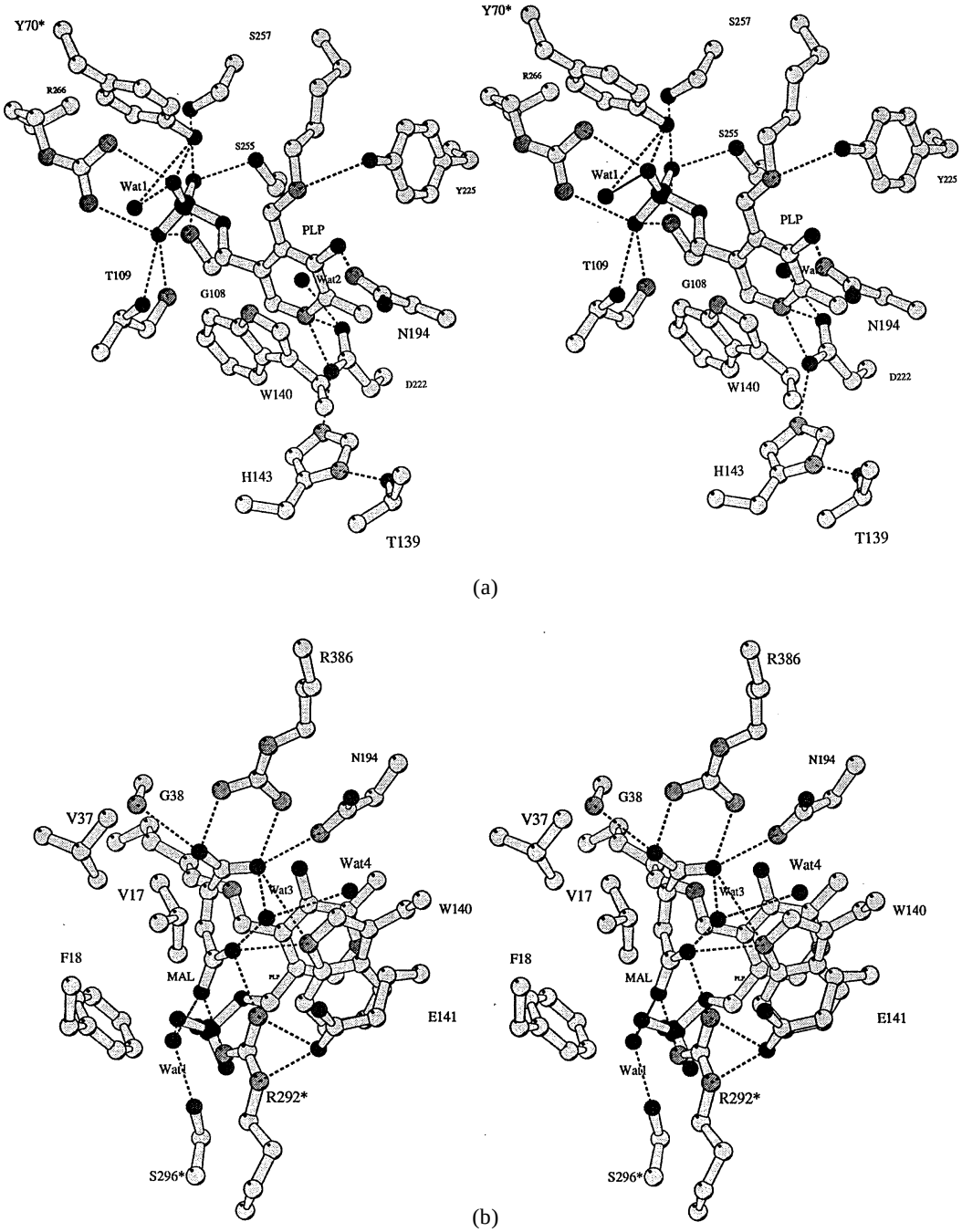

Figure 6. Stereoview of the cAATase active site. The gray level parallels the atomic number of the atoms. Broken lines indicate hydrogen bonds. (a) Coenzyme binding patch. Oxygen atoms of the phosphate group of the cofactor form multiple hydrogen bonds with the protein side-chains. The O-3' atom of the cofactor forms a hydrogen bond with the $N^{\delta 1}$ atom of Asn194, rather than with the hydroxyl group of Tyr225, as observed in mAATase (Jansonius & Vincent, 1987). (b) Inhibitor-binding site. The carboxylate groups of maleate form a network of hydrogen bonds with the surrounding hydrophilic side-chains. The hydrophobic side-chains of Val17, Phe18 and Val37 close the the inhibitor binding pocket at the top.

0.54 Å, respectively. Therefore, structural differences between the subunits are located mainly in the small domain. Visual analysis of the superimposed subunits indicates that the asymmetric lattice contacts induce slight (less than 0.5°) relative rotations of helix 1 (residues 16 to 26) and the C-terminal part of the long helix 12 (residues 313 to 344). It appears that the structural differences between the subunits have a lattice-induced character and do not have any functional significance. This conclusion is in agreement with the wealth of biochemical data that demonstrate equivalence of the two subunits of AATases (Christen & Metzler, 1985).

Amino acid sequence corrections

Two amino acid sequences are available for chicken cAATase. The first was determined using protein chemical methods (Shlyapnikov *et al*., 1979), whereas the second was deduced from the nucleotide sequence of the corresponding gene (Mattes *et al*., 1989). The two sequences disagree at positions 63, 121, 175, 232 and 234. After careful checks of the electron density maps, the sequence published by Mattes *et al*. (1989) was found to be more consistent with the crystallographic results. An arginine residue was built at position 121 during the chain tracing at 2.8 Å resolution (Borisov *et al*., 1985; Harutyunyan *et al*., 1985) before the nucleotide sequence became available. While Asp175, Ser232 and Asp234 suggested by the deduced sequence are well supported by their corresponding electron densities, Asp63 was accepted only on the basis of the deduced sequence, since the absolute choice between aspartate and asparagine side-chains could not be made independently for this residue, which is located in a flexible external loop.

Comparison with AATase structures from other sources

A deeper understanding of enzyme catalysis and the involvement of different parts of the enzyme molecule in it can be approached in two complementary ways. One is an exploration of the active site by means of site-directed mutagenesis. Alternatively, one can study the structural and functional properties of enzymes from different sources, the amino acid sequences of which have diverged through evolution. Both approaches have been successfully applied to many systems in the past. The ultimate goal of the present study was to expand the experimental basis for a structural comparison of AATases from different species or genes. A detailed comparison has not yet been carried out, but a tentative comparison of the chicken cAATase structure described here with the structures of the maleate complexes of chicken mAATase (Jansonius & Vincent, 1987; J. N. Jansonius *et al*., unpublished results) and eAATase (Jäger *et al*., 1994) revealed some unexpected differences (Malashkevich *et al*., 1991). Both chicken cAATase and mAATase adopt the closed conformation in the presence of maleate, but the degree of closure in cAATase is much smaller. A total rotation of 13° of the small domain towards the active site has been observed in mAATase upon transition from the open to the closed conformation (Jansonius & Vincent, 1987; Picot *et al*., 1991; McPhalen *et al*., 1992*b*). In the cAATase closed conformation the small domain is intermediate between its positions in the open and closed mAATase structures. This presumably explains the much higher affinity of cAATase for the five-carbon substrates, glutamate and 2-oxoglutarate. Greater domain closure leads to tighter packing of the side-chains (including Val37) around the substrate in the active site of mAATase, compared with the other isozymes, and this correlates well with lower affinity of this enzyme for five-carbon substrates. All three AATases bind four-carbon substrates almost equally well. Interestingly, the distance between the guanidinium groups of Arg386 and Arg292* is not influenced by the different degrees of closure in the maleate complexes of mAATase and cAATase. The latter in eAATase is intermediate between cAATase and mAATase.

The second important difference concerns the conformation of the coenzyme. In mAATase the O-5' atom of the phosphate ester of PLP is placed in front of the pyridine ring (in the view of Figure 6(a)), while in cAATase and eAATase it is behind the ring. This difference in conformation of PLP, caused probably by amino acid substitutions of residues interacting with the PLP-phosphate group (Gly107 and Ser257 in cAATase and eAATase, which are replaced by Ser and Ala, respectively, in mAATase), can influence the energetics of the pyridine ring rotations in the transaldimination reaction (Christen & Metzler, 1985).

The third difference concerns the environment of the side-chain of Arg292*, which plays a key role in recognition of the side-chain of dicarboxylic substrates and inhibitors in all AATases. AATases are known to transaminate also aromatic substrates with reasonable efficiency (in the order

Table 5

Selected active site interatomic distances for the cAATase maleate complex

Source atom	Target atom	Distance (Å)	Source atom	Target atom	Distance (Å)
N^{ζ} PLP	O-3'PLP	2.59 (2.67)[a]		$N^{\eta 2}$ Arg266	2.85 (2.83)
N1 PLP	$O^{\delta 1}$ Asp222	3.18 (3.27)		$O^{\gamma 1}$ Thr109	2.83 (2.76)
	$O^{\delta 2}$ Asp222	2.56 (2.64)	$O^{\delta 1}$ MAL	$N^{\eta 1}$ Arg292*	2.66 (2.74)
O-3'PLP	$N^{\delta 1}$ Asn194	3.11 (2.94)	$O^{\delta 2}$ MAL	$N^{\epsilon 1}$ Trp140	2.80 (2.88)
OP1 PLP	O^{γ} Ser257	2.65 (2.67)		$N^{\eta 2}$ Arg292*	2.89 (2.91)
	N Gly108	2.90 (2.91)		O Wat9	2.80 (2.79)
	O^{γ} Ser255	2.70 (2.71)	OT2 MAL	$N^{\epsilon 1}$ Trp140	3.24 (3.44)
OP2 PLP	$N^{\eta 1}$ Arg266	3.22 (3.37)		$N^{\delta 1}$ Asn194	2.93 (3.13)
	O^{η} Tyr70*	2.64 (2.49)		$N^{\eta 1}$ Arg386	2.92 (2.87)
	O Wat1	2.65 (2.57)	OT1 MAL	N Gly38	2.86 (2.86)
OP3 PLP	N Gly108	3.25 (3.15)		$N^{\eta 2}$ Arg386	2.92 (2.74)
	N Thr109	2.89 (2.92)			

[a] Distances in the second subunit are given in parentheses. MAL, maleate.

eAATase > mAATase > cAATase). How this is possible in the presence of Arg292* in this pocket remains unexplained. We found a marked charge redistribution in the immediate environment of Arg292* in the active sites of different AATases, mainly due to mutations at positions 15, 141 and 288. These mutations might, in an as yet unknown way, influence the behavior of the Arg292* side-chain upon binding of aromatic substrates.

Conclusions

The structural asymmetry observed for the chicken cAATase dimer in the present crystal form is not unique. Similar phenomena, be it of a lesser degree, were observed in several crystal forms of mAATase (McPhalen *et al*., 1992*a*; Hohenester & Jansonius, 1994), as well as in monoclinic crystals of eAATase (Jäger *et al*., 1994). This asymmetry is apparently induced by the crystal lattice. In solution, AATase was shown to be a symmetric homodimer with independently and identically behaving active sites. Additional evidence for identity of the two AATase subunits comes from the ability of mAATase to form orthorhombic crystals in which the two subunits are related by exact crystallographic symmetry (Jansonius & Vincent, 1987; Picot *et al*., 1991; McPhalen *et al*., 1992*b*). In solution, a significant fraction of mAATase molecules exists in partially or fully open conformations, even in the presence of saturating concentrations of the inhibitor maleate (Malashkevich *et al*., 1993). This phenomenon, which might be general for all AATases, discloses the domain closure mechanism as an equilibrium shift rather than a rigid switch between the two conformations. Subunit B in the cAATase structure presented here forms only one inter-dimer, i.e. crystal-packing, hydrogen bond in the crystal and therefore can be expected to behave essentially as in solution. The diffuse density observed in the small domain of subunit B, which indicates a high level of conformational flexibility, is in agreement with this conclusion. Subunit A, which forms multiple lattice contacts, is fixed in the unique closed conformation.

The structure of chicken cAATase represents the third AATase structure refined at a resolution higher than 2 Å, the others being chicken mAATase (McPhalen *et al*., 1992*a*) and eAATase (Okamoto *et al*., 1994). The overall fold and the secondary structure assignment of cAATase are very similar to those of the chicken mitochondrial enzyme (Jansonius & Vincent, 1987; McPhalen *et al*., 1992*a,b*). However, some interesting differences exist in the structure of the active site and in the coenzyme conformation. The published structures of different AATases provide a good basis for their detailed comparison, which will be given at a later time (V.N.M. & J. N. Jansonius, unpublished results).

The coordinates of the refined structure have been deposited with the Brookhaven Protein Data Bank, Chemistry Department, Brookhaven National Laboratory, Upton, NY, from which copies are available (entry code 2CST).

Materials and Methods

Crystallization

The enzyme was purified as described by Kochkina *et al*. (1978). The orthorhombic crystals were grown from a 17% (w/v) PEG solution buffered with 40 mM sodium maleate as described by Malashkevich & Sinitzina (1991). They belong to space group $P2_12_12_1$ with unit cell dimensions $a = 56.4$ Å, $b = 126.0$ Å and $c = 124.3$ Å. The asymmetric unit of these crystals contains one dimer of cAATase. The crystals grow to a maximum size of 0.6 mm × 0.7 mm × 2.5 mm, but smaller crystals of typical size 0.3 mm × 0.3 mm × 1.5 mm were used for data collection at the synchrotron beam.

Data collection and processing

Three-dimensional data were initially collected using a four-circle Syntex $P2_1$ diffractometer with Ni-monochromatized CuKα radiation. The ω-scan method was used for data collection in spherical shells of resolution. In order to shorten the time required for data collection, fast background measurements (one to two seconds) were used with peak measurement times of one to three minutes. A six-parameter function was used for smoothing the statistically unreliable measurements of the background (Brayer *et al.*, 1978). The crystals studied here were more resistant to radiation damage than the previously used high-salt crystal form (Borisov *et al*., 1985; Harutyunyan *et al*., 1985). A total of 41,500 unique reflections between 100.0 and 2.23 Å resolution was collected using only two crystals. The elongated morphology of the crystals allowed exposure of two different sample volumes per crystal. The maximum tolerated intensity decay for a selected group of reflections, due to radiation damage, was 15%. The R_{sym} value after absorption, Lorentz and polarization corrections was 4.5%.

Synchrotron diffraction data were collected on the X11 beamline at the EMBL Out-station, DESY, Hamburg. The radiation was monochromatized and focused in the horizontal plane with a germanium crystal. The vertical focusing was effected by a segmented mirror mounted on a bendable bench. The wavelength used was 1.06 Å. Data were recorded using an imaging plate scanner controlled by a MicroVAX computer. Three sets of diffraction data were collected for high (1.9 Å) and low (2.6 Å) resolution, and also for a blind region (1.9 Å). Subsequent calculations were carried out using the CCP4 suite of programs (SERC Daresbury Laboratory, 1986). The raw data were processed with a modified version of the MOSFLM film processing package (Leslie, 1991). The merging of the observed intensities to give a unique set of reflections was carried out with the programs ROTAVATA/AGROVATA. Intensities were converted to structure factor amplitudes with the program TRUNCATE. The total number of reflections measured was 310,873, comprising 265,110 fully recorded and 45,763 partially recorded. These reduced to a set of 69,642 independent reflections, corresponding to 98.5% of the unique data to 1.9 Å resolution. The overall R_{sym} for the symmetry-equivalent reflections for all three data sets was 9.5%. The cumulative percentages of reflections with intensity greater than one, two and three standard deviations were 91.0, 85.7 and 80.9%, respectively.

Structure determination

The structure of the new orthorhombic crystal form was solved by molecular replacement using the partially refined 2.8 Å resolution structure of the high-salt crystal form (Borisov *et al*., 1985; Harutyunyan *et al*., 1985) as a search model. The orientation of the molecule in the new unit cell was found using the Crowther fast rotation function (Crowther, 1972). The highest peak of the cross-rotation function calculated with integration radius of 20 Å and a resolution range from 20 to 3.4 Å corresponded to Eulerian angles α, β, γ of 10.0°, 0.0° and 127.5°, respectively. The next highest peak of the cross-rotation function was 25% of the correct solution. The orientation of the dimer obtained from the cross-rotation is in agreement with a self-rotation function calculated for the new crystal form. The molecular 2-fold axis lies in the *ab* plane, as in the high salt crystal form, but it is rotated by 42.5° relative to the direction in the latter. The center of mass of the molecule was placed at the point with coordinates $x = 0.869$, $y = 0.055$ and $z = 0.413$ in accordance with the position of the highest peak found on the translation function map. Analysis of the packing function (Vagin, 1983) and visual inspection of the unit cell content showed no bad contact between symmetry-related molecules oriented and positioned according to the molecular replacement solution. The initial value of the crystallographic *R*-factor at this stage, calculated for data ranging from 10.0 to 3.4 Å, was 49.4%.

Rigid body refinement

The program CORELS (Sussman *et al*., 1977) was used to refine the orientational and the positional parameters of the protein molecule. In the first cycle, the positions and the orientations of both subunits of cAATase were refined separately. Then, each subunit was divided into six rigid bodies. The first includes the residues of the N-terminal ''arm'' (residues 2 to 14), the second (residues 15 to 50) and the sixth (residues 360 to 412) groups comprise the residues of the small domain. The fourth group (residues 76 to 300) comprises the residues of the large domain and the two remaining groups comprise the residues of the domain interface. Several refinement cycles resulted in an *R*-factor of 42.0% in the resolution range from 8.0 to 5.0 Å. Subsequent refinement of the positional parameters and the torsion angles of the 822 amino acid residues treated as a chain of rigid bodies resulted in an *R*-factor of 24.9% in the resolution range from 7.0 to 4.0 Å.

Restrained refinement

Restrained least-squares refinement was carried out with the programs PROLSQ (Hendrickson, 1985) and TNT (Tronrud *et al*., 1987). Inspection and interpretation of the electron density maps and rebuilding of the model were carried out on a PS330 graphics display system using the software package FRODO (Jones, 1978) modified by Pflugrath *et al*. (1984). The starting model for refinement was that obtained from the rigid body refinement. No 2-fold restraint was imposed. In the first few cycles, after every manual rebuild of the model or addition of new water molecules, only medium-resolution data between 7.0 and 2.7 Å were included in the refinement. Higher-resolution data were gradually added after careful examination of the model, using electron density maps with phases computed from the model and with coefficients $(2F_{obs} - F_{calc})$, α_{calc} and $(F_{obs} - F_{calc})$, α_{calc}. σ_A weights (Read, 1986) were used throughout in refinement and map calculations. The crystallographic *R*-value after refinement against diffractometer data was 16.1% for 37,500 reflections greater than 1σ in the resolution range from 7.0 to 2.23 Å. After the synchrotron data became available they were used for further refinement. The initial *R*-factor was 31% for the same resolution range. After additional positional and individual *B*-factor refinement with TNT accompanied by rebuilding of the model and positioning of the water molecules, refinement converged at a final value of 17.5% for all 67,544 reflections in the resolution range from 6.0 to 1.9 Å. The final refinement statistics are given in Table 1.

Acknowledgements

We thank Nina Sinitzina for providing pure enzyme. We are very grateful to Dr Johan N. Jansonius for valuable discussions and for the hospitality provided to V.N.M. during his three months stay at the Biozentrum. We thank Dr Johan N. Jansonius and Erhard Hohenester for critical reading of the manuscript. This project was supported in part by EMBO fellowship ASTF 5947 to V.N.M.

References

Arnone, A., Rogers, P. H., Hyde, C. C., Briley, P. D., Metzler, C. M. & Metzler, D. E. (1985). Pig cytosolic aspartate aminotransferase: the structure of the internal aldimine, external aldimine, and ketimine and of the β-subform. In *Transaminases* (Christen, P. & Metzler, D. E., eds), pp. 138–155, John Wiley & Sons, New York.

Borisov, V. V., Borisova, S. N., Kachalova, G. S., Sosfenov, N. I. & Vainstein, B. K. (1985). X-ray studies of chicken cytosolic aspartate aminotransferase. In *Transaminases* (Christen, P. & Metzler, D. E., eds), pp. 155–164, John Wiley & Sons, New York.

Brayer, G. D., Delbare, T. J. & James, M. N. G. (1978). Molecular structure of crystalline *Streptomyces griseus* protease A at 2.8 Å resolution. I. Crystallization data collection and structure analysis. *J. Mol. Biol.* **124**, 243–259.

Christen, P. & Metzler, D. E. (1985) Editors of *Transaminases*, J. Wiley and Sons, New York.

Crawford, J. L., Lipscomb, W. N. & Schellman, C. G. (1973). The reverse turn as a polypeptide conformation in globular proteins. *Proc. Nat. Acad. Sci., U.S.A.* **70**, 538–542.

Cronin, C. N. & Kirsch, J. F. (1988). Role of arginine-292 in the substrate specificity of aspartate aminotransferase as examined by site-directed mutagenesis. *Biochemistry*, **27**, 4572–4579.

Crowther, R. A. (1972). The fast rotation function. In *Molecular Replacement Method* (M. G. Rossman, ed.), pp. 173–185, Gordon and Breach, New York.

Cruickshank, D. W. J. (1949). The accuracy of electron-density maps in X-ray analysis with special reference to dibenzyl. *Acta Crystallogr.* **2**, 65–82.

Fasella, P. & Haslam, G. G. (1967). A temperature jump study of aspartate aminotransferase. A reinvestigation. *Biochemistry*, **6**, 1798–1804.

Ford, G. C., Eichele, G. & Jansonius, J. N. (1980). Three-dimensional structure of a pyridoxal-phosphate-dependent enzyme, mitochondrial aspartate aminotransferase. *Proc. Nat. Acad. Sci., U.S.A.* **77**, 2559–2563.

Goldberg, J. M., Swanson, R. V., Goodman, H. S. & Kirsch,

J. F. (1991). The tyrosine-225 to phenylalanine mutation of *Escherichia coli* aspartate aminotransferase results in an alcaline transition in the spectrophotometric and kinetic pK_a values and reduced values of k_{cat} and k_m. *Biochemistry,* **30**, 305–312.

Graf-Hausner, U., Wilson, K. J. & Christen, P. (1983). The covalent structure of mitochondrial aspartate aminotransferase from chicken. *J. Biol. Chem.* **258**, 8813–8826.

Harutyunyan, E. G., Malashkevich, V. N., Kochkina, V. M. & Torchinsky, Y. M. (1985). Three-dimensional structure of the complex of chicken cytosolic aspartate aminotransferase with 2-oxoglutarate. In *Transaminases* (Christen, P. & Metzler, D. E., eds), pp. 164–173, John Wiley & Sons, New York.

Hayashi, H., Inoue, Y., Kuramitsu, S. & Kagamiyama, H. (1991). *Escherichia coli* aspartate aminotransferase: effects of site-specific mutations on substrate binding and catalysis. In *Enzymes Dependent on Pyridoxal Phosphate and Other Carbonyl Compounds as Cofactors* (Fukui, T., Kagamiyama, H., Soda, K. & Wada, H., eds), pp. 183–186, Pergamon Press, Oxford.

Hendrickson, W. A. (1985). Stereochemically restrained refinement of macromolecular structures. *Methods Enzymol.* **115**, 252–270.

Hohenester, E. & Jansonius, J. N. (1994). Crystalline mitochondrial aspartate aminotransferase exists in only two conformations. *J. Mol. Biol.* **236**, 963–968.

Inoue, K., Kuramitsu, S., Okamoto, A., Hirotsu, K., Higuchi, T., Morino, Y. & Kagamiyama, H. (1991). Tyr-225 in aspartate aminotransferase: contribution of the hydrogen bond between Tyr-225 and coenzyme to the catalytic reaction. *J. Biochem.* **109**, 570–576.

Izard, T. (1990). Structure determination of porcine mitochondrial aspartate aminotransferase in the closed conformation. Diploma thesis, University of Basel.

Jäger, J., Moser, M., Sauder, U. & Jansonius, J. N. (1994). Crystal structures of *Escherichia coli* aspartate aminotransferase in two conformations. Comparison of an unliganded and two liganded closed forms. *J. Mol. Biol.* **239**, 285–305.

Jansonius, J. N. & Vincent, M. G. (1987). Structural basis for catalysis by aspartate aminotransferase. In *Biological Macromolecules and Assemblies* (Jurnak, F. A. & McPherson, A., eds), vol. 3, pp. 187–285, John Wiley & Sons, New York.

Jansonius, J. N., Eichele, G. Ford, G. C., Picot, D., Thaller, C. & Vincent, M. G. (1985). Spatial structure of mitochondrial aspartate aminotransferase. In *Transaminases* (Christen, P. & Metzler, D., eds), pp. 109–137, John Wiley & Sons, New York.

Jones, T. A. (1978). Interactive computer graphics: FRODO. *Methods Enzymol.* **115**, 157–171.

Kabsch, W. & Sander, C. (1983). Dictionary of protein secondary structure: pattern recogniton of hydrogen bonded and geometrical features. *Biopolymers,* **22**, 2577–2637.

Kintanar, A., Metzler, C. M., Metzler, D. E. & Scott, R. D. (1991). NMR observation of exchangeable protons of pyridoxal phosphate and histidine residue in cytosolic aspartate aminotransferase. *J. Biol. Chem.* **266**, 17222–17229.

Kirsch, J. F., Eichele, G., Ford, G. C., Vincent, M. G., Jansonius, J. N., Gehzing, H. & Christen, P. (1984). Mechanism of action of aspartate aminotransferase proposed on the basis of its spatial structure. *J. Mol. Biol.* **174,** 497–525.

Kochkina, V. M., Azaryan, A. V., Mekhanik, M. L., Sinitzina, N. I. & Torchinsky, Yu. M. (1978). Purification of aspartate transaminase from chicken heart cytosol. *Biokhimia (Moscow),* **43**, 1478–1484.

Kuramitsu, S., Yano, T., Inoue, K., Hiromi, K., Tanase, S., Morino, Y. & Kagamiyama, H. (1991). Asp222, His143 and Tyr70 in *Escherichia coli* aspartate aminotransferase. In *Enzymes Dependent on Pyridoxal Phosphate and Other Carbonyl Compounds as Cofactors* (Fukui, T., Kagamiyama, H., Soda, K. & Wada, H., eds), pp. 179–181, Pergamon Press, Oxford.

Leslie, A. G. W. (1991). Recent changes to the MOSFLM package for processing film and image plate data. *CCP4 and ESF-EACMB Newsletter on Protein Crystallograph*. Aavailable from librarian, SERC Laboratory, Daresbury Warrington WA4 4AD, England.

Luzzati, V. (1952). Traitement statistique des erreurs dans la determination des structures cristallines. *Acta Crystallogr.* **5**, 802–819.

Malashkevich, V. N. & Sinitzina, N. I. (1991). New crystal form of cytosolic chicken aspartate aminotransferase suitable for high-resolution X-ray analysis. *J. Mol. Biol.* **221**, 61–63.

Malashkevich, V. N., Torchinsky, Yu. M., Strokopytov, B. V., Borisov, V. V., Genovesio-Taverne, J.-C. & Jansonius, J. N. (1991). The structure differences between chicken cytosolic and mitochondrial aspartate aminotransferases. In *Enzymes Dependent on Pyridoxal Phosphate and Other Carbonyl Compounds as Cofactors* (Fukui, T., Kagamiyama, H., Soda, K. & Wada, H., eds), pp. 99–105, Pergamon Press, Oxford.

Malashkevich, V. N., Toney, M. D. & Jansonius, J. N. (1993). Crystal structures of true enzymatic reaction intermediates: aspartate and glutamate ketimines in aspartate aminotransferase. *Biochemistry,* **32**, 13451–13462.

Malcolm, B. A. & Kirsch, J. F. (1985). Site-directed mutagenesis of aspartate aminotransferase from *E. coli*. *Biochem. Biophys. Res. Commun.* **132**, 915–921.

Martinez-Carrion, M. (1975). ^{31}P nuclear-magnetic-resonance studies of pyridoxal and pyridoxamine phosphates. Interaction with cytoplasmic aspartate transaminase. *Eur. J. Biochem.* **54**, 39–43.

Mattes, U., Jaussi, R., Ziak, M., Juretic, N., Lindenmann, J.-M. & Christen, P. (1989). Structure of cDNA of cytosolic aspartate aminotransferase of chicken and its expression in *E. coli. Biochimie,* **71**, 411–416.

McPhalen, C., Vincent, M. G. & Jansonius, J. N. (1992*a*). X-ray structure refinements and comparisons among three forms of mitochondrial aspartate aminotransferase. *J. Mol. Biol.* **225**, 495–517.

McPhalen, C., Vincent, M. G., Picot, D., Jansonius, J. N., Lesk, A. M. & Chothia, C. (1992*b*). Domain closure in mitochondrial aspartate aminotransferase. *J. Mol. Biol.* **227**, 197–213.

Mehta, P. K., Hale, T. I. & Christen, P. (1989). Evolutionary relationships among aminotransferases: tyrosine aminotransferase and aspartate aminotransferase are homologous proteins. *Eur. J. Biochem.* **186**, 249–253.

Metzler, D. E. (1979). Tautomerism in pyridoxal phosphate and in enzymatic catalysis. *Advan. Enzymol.* **50**, 1–40.

Mitchell, B. O., Thornton, J. M., Singh, J. & Price, S. L. (1992). Towards the understanding of the arginine-aspartate interaction. *J. Mol. Biol.* **226**, 251–262.

Morris, A. L., MacArthur, M. W., Hutchinson, E. G. & Thornton, J. M. (1992). Stereochemical quality of protein structure coordinates. *Proteins: Struct. Funct. Genet.* **12**, 345–364.

Okamoto, A., Higuchi, T., Hirotsu, K., Kuramitsu, S. & Kagamiyama, H. (1994). X-ray crystallographic study

of pyridoxal 5'-phosphate-type aspartate aminotransferases from *Escherichia coli* in open and closed form. *J. Biochem. (Tokyo)*, **116**, 95–107.

Pflugrath, J. W., Saper, M. A. & Quiocho, F. A. (1984). New generation graphics system for molecular modelling. In *Methods and Applications in Crystallographic Computing* (Hall, S. & Ashida, T., eds), pp. 404–407, Clarendon Press, Oxford.

Picot, D., Sandmeier, E., Thaller, C., Vincent, M. G., Christen, P. & Jansonius, J. (1991). The open/closed equilibrium of aspartate aminotransferase: studies in the crystalline state and with a fluorescent probe in solution. *Eur. J. Biochem.* **196**, 329–341.

Ramakrishnan, C. & Ramachandran, G. N. (1965). Stereochemical criteria for polypeptide and protein chain confromations. II. Allowed conformations for a pair of peptide units. *Biophys. J.* **5**, 909–933.

Read, R. J. (1986). Improved Fourier coefficients for maps using phases from partial structures with errors. *Acta Crystallogr. sect. A*, **42**, 140–149.

Richardson, J. S. (1981). The anatomy and taxonomy of protein structure. *Advan. Protein Chem.* **34**, 167–339.

Schnackerz, K. D. (1984). Phosphorus-31 nuclear magnetic resonance study on cytoplasmic aspartate aminotransferase from pig heart. A reinvestigation. *Biophys. Biochim. Acta*, **789**, 241–244.

Schnackerz, K. D., Wahler, G., Vincent, M. G. & Jansonius, J. N. (1989). Evidence that ^{31}P NMR is a sensitive indicator of small conformational changes in the coenzyme of aspartate aminotransferase. *Eur. J. Biochem.* **185**, 525–531.

SERC Daresbury Laboratory (1986). CCP4. *A Suite of Programs for Protein Crystallography*. SERC Daresbury Laboratory, Warrington, UK.

Shlyapnikov, S. V., Myasūikov, A. N., Severin, E. S., Myagkova, M. A., Torchinsky, Y. M. & Braunstein, A. E. (1979). Primary structure of cytoplasmic aspartate aminotransferase from chicken heart and its homology with pig heart isoenzymes. *FEBS Letters*, **106,** 385–388.

Smith, D. L., Almo, S. C., Toney, M. D. & Ringe, D. (1989). 2.8 Å resolution crystal structure of an active-site mutant of aspartate aminotransferase from *Escherichia coli*. *Biochemistry*, **28**, 8161–8167.

Sussman, J. L., Holbrook, S. R., Church, G. M. & Kim, S.-H. (1977). A structure-factor least-squares refinement procedure for macromolecular structures using constrained and restrained parameters. *Acta Crystallogr. sect. A*, **33,** 800–804.

Toney, M. D. & Kirsch, J. F. (1987). Tyrosine 70 increases the coenzyme affinity of aspartate aminotransferase. A site directed mutagenesis study. *J. Biol. Chem.* **262**, 12403–12405.

Toney, M. D. & Kirsch, J. F. (1991). The K258R mutant of aspartate aminotransferase stabilizes the quinonoid intermediate. *J. Biol. Chem.* **266**, 23900–23903.

Tronrud, D. E., Ten Eyck, L. F. & Matthews, B. W. (1987). An efficient general-purpose least-squares refinement program for macromolecular structures. *Acta Crystallogr. sect. A*, **43**, 489–501.

Vagin, A. A. (1983). Use of noncrystallographic symmetry in structural crystallography of proteins. PhD thesis, Institute of Crystallography, Moscow.

Yano, T., Kuramitsu, S., Tanase, S., Morino, Y., Hiromi, K. & Kagamiyama, H. (1991). The role of His143 in the catalytic mechanism of *Escherichia coli* aspartate aminotransferase. *J. Biol. Chem.* **266**, 6079–6085.

Yano, T., Kuramitsu, S., Tanase, S., Morino, Y. & Kagamiyama, H. (1992). The role of Asp222 in the catalytic mechanism of *Escherichia coli* aspartate aminotransferase. *Biochemistry*, **31**, 5878–5887.

Ziak, M., Jäger, J., Malashkevich, V. N., Gehring, H., Jaussi, R. & Christen, P. (1993). Mutant aspartate aminotransferase (K258H) without pyridoxal-5'-phosphate-binding lysine residue. Structural and catalytic properties. *Eur. J. Biochem.* **187**, 329–333.

Edited by R. Huber

(Received 5 September 1994; accepted 13 December 1994)